



HAL
open science

Measurement and interpretation of the W-pair cross-section in e^+e^- interactions at 161 GeV

P. Abreu, W. Adam, T. Adye, P. Adzic, I. Ajinenko, G D. Alekseev, R. Alemany, P P. Allport, S. Almeded, U. Amaldi, et al.

► **To cite this version:**

P. Abreu, W. Adam, T. Adye, P. Adzic, I. Ajinenko, et al.. Measurement and interpretation of the W-pair cross-section in e^+e^- interactions at 161 GeV. Physics Letters B, 1997, 397, pp.158-170. 10.1016/S0370-2693(97)00226-8 . in2p3-00001131

HAL Id: in2p3-00001131

<https://in2p3.hal.science/in2p3-00001131v1>

Submitted on 17 Nov 1998

HAL is a multi-disciplinary open access archive for the deposit and dissemination of scientific research documents, whether they are published or not. The documents may come from teaching and research institutions in France or abroad, or from public or private research centers.

L'archive ouverte pluridisciplinaire **HAL**, est destinée au dépôt et à la diffusion de documents scientifiques de niveau recherche, publiés ou non, émanant des établissements d'enseignement et de recherche français ou étrangers, des laboratoires publics ou privés.

Measurement and interpretation of the W -pair cross-section in e^+e^- interactions at 161 GeV

DELPHI Collaboration

Abstract

In 1996 LEP ran at a centre-of-mass energy of 161 GeV, just above the threshold of W -pair production. DELPHI accumulated data corresponding to an integrated luminosity of 9.93 pb^{-1} , and observed 29 events that are considered as candidates for W -pair production. From these, a cross-section for the doubly resonant $e^+e^- \rightarrow WW$ process of $3.67^{+0.97}_{-0.85} \pm 0.19 \text{ pb}$ has been measured. Within the Standard Model, this cross-section corresponds to a mass of the W -boson of $80.40 \pm 0.44 \text{ (stat.)} \pm 0.09 \text{ (syst.)} \pm 0.03 \text{ (LEP)} \text{ GeV}/c^2$. Alternatively, if m_W is held fixed at its current value determined by other experiments, the observed cross-section is used to obtain limits on trilinear WWV ($V \equiv \gamma, Z$) couplings.

(To be submitted to Physics Letters B)

P.Abreu²¹, W.Adam⁵⁰, T.Adye³⁷, P.Adzic¹¹, I.Ajinenko⁴², G.D.Alekseev¹⁶, R.Aleman⁴⁹, P.P.Allport²², S.Almehed²⁴, U.Amaldi⁹, S.Amato⁴⁷, A.Andrezza²⁸, M.L.Andrieux¹⁴, P.Antilogus⁹, W-D.Apel¹⁷, B.Åsman⁴⁴, J-E.Augustin²⁵, A.Augustinus³¹, P.Baillon⁹, P.Bambade¹⁹, F.Barao²¹, M.Barbi⁴⁷, D.Y.Bardin¹⁶, G.Barker⁹, A.Baroncelli⁴⁰, O.Barring²⁴, J.A.Barrio²⁶, W.Bartl⁵⁰, M.J.Bates³⁷, M.Battaglia¹⁵, M.Baubillier²³, J.Baudot³⁹, K-H.Becks⁵², M.Begalli⁶, P.Beilliere⁸, Yu.Belokopytov^{9,53}, K.Belous⁴², A.C.Benvenuti⁵, M.Berggren⁴⁷, D.Bertini²⁵, D.Bertrand², M.Besancon³⁹, F.Bianchi⁴⁵, M.Bigli⁴⁵, M.S.Bilenky¹⁶, P.Billoir²³, M-A.Bizouard¹⁹, D.Bloch¹⁰, M.Blume⁵², T.Bolognese³⁹, M.Bonesini²⁸, W.Bonivento²⁸, P.S.L.Booth²², C.Bosio⁴⁰, O.Botner⁴⁸, E.Boudinov³¹, B.Bouquet¹⁹, C.Bourdarios¹⁹, T.J.V.Bowcock²², M.Bozzo¹³, P.Branchini⁴⁰, K.D.Brand³⁶, T.Brenke⁵², R.A.Brenner¹⁵, C.Bricman², R.C.A.Brown⁹, P.Bruckman¹⁸, J-M.Brunet⁸, L.Bugge³³, T.Buran³³, T.Burgsmueller⁵², P.Buschmann⁵², S.Cabrera⁴⁹, M.Caccia²⁸, M.Calvi²⁸, A.J.Camacho Rozas⁴¹, T.Camporesi⁹, V.Canale³⁸, M.Canepa¹³, K.Cankocak⁴⁴, F.Cao², F.Carena⁹, L.Carroll²², C.Caso¹³, M.V.Castillo Gimenez⁴⁹, A.Cattai⁹, F.R.Cavallo⁵, V.Chabaud⁹, Ph.Charpentier⁹, L.Chaussard²⁵, P.Checchia³⁶, G.A.Chelkov¹⁶, M.Chen², R.Chierici⁴⁵, P.Chliapnikov⁴², P.Chochula⁷, V.Chorowicz²⁵, J.Chudoba³⁰, V.Cindro⁴³, P.Collins⁹, R.Contri¹³, E.Cortina⁴⁹, G.Cosme¹⁹, F.Cossutti⁴⁶, J-H.Cowell²², H.B.Crawley¹, D.Crennell³⁷, G.Crosetti¹³, J.Cuevas Maestro³⁴, S.Czellar¹⁵, E.Dahl-Jensen²⁹, J.Dahm⁵², B.Dalmagne¹⁹, M.Dam²⁹, G.Damgaard²⁹, P.D.Dauncey³⁷, M.Davenport⁹, W.Da Silva²³, C.Defoix⁸, A.Deghorain², G.Della Ricca⁴⁶, P.Delpierre²⁷, N.Demaria³⁵, A.De Angelis⁹, W.De Boer¹⁷, S.De Brabandere², C.De Clercq², C.De La Vaissiere²³, B.De Lotto⁴⁶, A.De Min³⁶, L.De Paula⁴⁷, C.De Saint-Jean³⁹, H.Dijkstra⁹, L.Di Ciaccio³⁸, A.Di Diodato³⁸, A.Djannati⁸, J.Dolbeau⁸, K.Doroba⁵¹, M.Dracos¹⁰, J.Drees⁵², K.-A.Drees⁵², M.Dris³², J-D.Durand^{25,9}, D.Edsall¹, R.Ehret¹⁷, G.Eigen⁴, T.Ekelof⁴⁸, G.Ekspog⁴⁴, M.Elsing⁹, J-P.Engel¹⁰, B.Erzen⁴³, E.Falk²⁴, G.Fanourakis¹¹, D.Fassouliotis⁴⁶, M.Feindt⁹, P.Ferrari²⁸, A.Ferrer⁴⁹, S.Fichet²³, T.A.Filippas³², A.Firestone¹, P.-A.Fischer¹⁰, H.Foeth⁹, E.Fokitis³², F.Fontanelli¹³, F.Formenti⁹, B.Franek³⁷, P.Frenkiel³⁷, A.G.Frodesen⁴, R.Fruhworth⁵⁰, F.Fulda-Quenzer¹⁹, J.Fuster⁴⁹, A.Galloni²², D.Gamba⁴⁵, M.Gandelman⁴⁷, G.Garcia⁴⁹, J.Garcia⁴¹, C.Gaspar⁹, U.Gasparini³⁶, Ph.Gavillet⁹, E.N.Gaziz³², D.Gele¹⁰, J-P.Gerber¹⁰, L.Gerdykov⁴², R.Gokiel⁵¹, B.Golob⁴³, P.Goncalves²¹, G.Gopal³⁷, L.Gorn¹, M.Gorski⁵¹, Yu.Gouz^{45,53}, V.Gracco¹³, E.Graziani⁴⁰, C.Green²², A.Grefrath⁵², P.Gris³⁹, G.Grosdidier¹⁹, K.Grzelak⁵¹, S.Gumenyuk⁴², P.Gunnarsson⁴⁴, M.Gunther⁴⁸, J.Guy³⁷, F.Hahn⁹, S.Hahn⁵², Z.Hajduk¹⁸, A.Hallgren⁴⁸, K.Hamacher⁵², F.J.Harris³⁵, V.Hedberg²⁴, R.Henriques²¹, J.J.Hernandez⁴⁹, P.Herquet², H.Herr⁹, T.L.Hessing³⁵, J.-M.Heuser⁵², E.Higon⁴⁹, H.J.Hilke⁹, T.S.Hill¹, S-O.Holmgren⁴⁴, P.J.Holt³⁵, D.Holthuizen³¹, S.Hoorelbeke², M.Houlden²², J.Hrube⁵⁰, K.Huet², K.Hultqvist⁴⁴, J.N.Jackson²², R.Jacobsson⁴⁴, P.Jalocha¹⁸, R.Janik⁷, Ch.Jarlskog²⁴, G.Jarlskog²⁴, P.Jarry³⁹, B.Jean-Marie¹⁹, E.K.Johansson⁴⁴, L.Jonsson²⁴, P.Jonsson²⁴, C.Joram⁹, P.Juillot¹⁰, M.Kaiser¹⁷, F.Kapusta²³, K.Karafasoulis¹¹, M.Karlsson⁴⁴, S.Katsanevas²⁵, E.C.Katsoufis³², R.Keranen⁴, Yu.Khokhlov⁴², B.A.Khomenko¹⁶, N.N.Khovanski¹⁶, B.King²², N.J.Kjaer³¹, O.Klapp⁵², H.Klein⁹, A.Klovning⁴, P.Kluit³¹, D.Knoblach¹⁷, P.Kokkinias¹¹, A.Konopliannikov⁴², M.Koratzinos⁹, K.Korcy¹⁸, V.Kostiukhine⁴², C.Kourkoumelis³, O.Kouznetsov^{13,16}, M.Krammer⁵⁰, C.Kreuter⁹, I.Kronkvist²⁴, Z.Krumstein¹⁶, W.Krupinski¹⁸, P.Kubinec⁷, W.Kucewicz¹⁸, K.Kurvinen¹⁵, C.Lacasta⁴⁹, I.Laktineh²⁵, J.W.Lamsa¹, L.Lanceri⁴⁶, D.W.Lane¹, P.Langefeld⁵², J-P.Laugier³⁹, R.Lauhakangas¹⁵, G.Leder⁵⁰, F.Ledroit¹⁴, V.Lefebure², C.K.Legan¹, A.Leisos¹¹, R.Leitner³⁰, J.Lemone², G.Lenzen⁵², V.Lepeltier¹⁹, T.Lesiak¹⁸, J.Libby³⁵, D.Liko⁹, R.Lindner⁵², A.Lipniacka⁴⁴, I.Lippi³⁶, B.Loerstad²⁴, J.G.Loken³⁵, J.M.Lopez⁴¹, D.Loukas¹¹, P.Lutz³⁹, L.Lyons³⁵, J.MacNaughton⁵⁰, G.Maehlum¹⁷, J.R.Mahon⁶, A.Maio²¹, T.G.M.Malmgren⁴⁴, V.Malychev¹⁶, J.Marco⁴¹, R.Marco⁴¹, B.Marechal⁴⁷, M.Margoni³⁶, J-C.Marin⁹, C.Mariotti⁹, A.Markou¹¹, C.Martinez-Rivero³⁴, F.Martinez-Vidal⁴⁹, S.Marti i Garcia²², J.Masik³⁰, F.Matorras⁴¹, C.Matteuzzi²⁸, G.Matthiae³⁸, M.Mazzucato³⁶, M.Mc Cubbin²², R.Mc Kay¹, R.Mc Nulty²², J.Medbo⁴⁸, M.Merk³¹, C.Meroni²⁸, S.Meyer¹⁷, W.T.Meyer¹, M.Michelotto³⁶, E.Migliore⁴⁵, L.Mirabito²⁵, W.A.Mitaroff⁵⁰, U.Mjoernmark²⁴, T.Moa⁴⁴, R.Moeller²⁹, K.Moenig⁹, M.R.Monge¹³, P.Morettini¹³, H.Mueller¹⁷, K.Muenich⁵², M.Mulders³¹, L.M.Mundim⁶, W.J.Murray³⁷, B.Muryn^{14,18}, G.Myatt³⁵, F.Naraghi¹⁴, F.L.Navarria⁵, S.Navas⁴⁹, K.Nawrocki⁵¹, P.Negri²⁸, W.Neumann⁵², N.Neumeister⁵⁰, R.Nicolaïdou³, B.S.Nielsen²⁹, M.Nieuwenhuizen³¹, V.Nikolaenko¹⁰, P.Niss⁴⁴, A.Nomerotski³⁶, A.Normand³⁵, W.Oberschulte-Beckmann¹⁷, V.Obraztsov⁴², A.G.Olshevski¹⁶, A.Onofre²¹, R.Orava¹⁵, G.Orazi¹⁰, K.Osterberg¹⁵, A.Ouraou³⁹, P.Paganini¹⁹, M.Paganoni^{9,28}, P.Pages¹⁰, R.Pain²³, H.Palka¹⁸, Th.D.Papadopoulou³², K.Papageorgiou¹¹, L.Pape⁹, C.Parkes³⁵, F.Parodi¹³, A.Passeri⁴⁰, M.Pegoraro³⁶, L.Peralta²¹, H.Pernegger⁵⁰, M.Pernicka⁵⁰, A.Perrotta⁵, C.Petridou⁴⁶, A.Petrolini¹³, H.T.Phillips³⁷, G.Piana¹³, F.Pierre³⁹, M.Pimenta²¹, T.Podobnik⁴³, O.Podobrin⁹, M.E.Pol⁶, G.Polok¹⁸, P.Poropat⁴⁶, V.Pozdniakov¹⁶, P.Privitera³⁸, N.Pukhaeva¹⁶, A.Pullia²⁸, D.Radojicic³⁵, S.Ragazzi²⁸, H.Rahmani³², J.Rames¹², P.N.Ratoff²⁰, A.L.Read³³, M.Reale⁵², P.Rebecchi¹⁹, N.G.Redaeli²⁸, M.Regler⁵⁰, D.Reid⁹, R.Reinhardt⁵², P.B.Renton³⁵, L.K.Resvanis³, F.Richard¹⁹, J.Richardson²², J.Ridky¹², G.Rinaudo⁴⁵, I.Ripp³⁹, A.Romero⁴⁵, I.Roncagliolo¹³, P.Ronchese³⁶, L.Roos²³, E.I.Rosenberg¹, P.Roudeau¹⁹, T.Rovelli⁵, V.Ruhlmann-Kleider³⁹, A.Ruiz⁴¹, K.Rybicki¹⁸, H.Saarikko¹⁵, Y.Sacquin³⁹, A.Sadovsky¹⁶, O.Sahr¹⁴, G.Sajot¹⁴, J.Salt⁴⁹, J.Sanchez²⁶, M.Sannino¹³, H.Schneider¹⁷, U.Schwickerath¹⁷, M.A.E.Schyns⁵², G.Sciolla⁴⁵, F.Scuri⁴⁶, P.Seager²⁰, Y.Sedykh¹⁶, A.M.Segar³⁵, A.Seitz¹⁷, R.Sekulin³⁷, L.Serbelloni³⁸, R.C.Shellard⁶, P.Siegrist^{9,39}, R.Silvestre³⁹, S.Simonetti³⁹, F.Simonetto³⁶, A.N.Sisakian¹⁶, B.Sitar⁷, T.B.Skaali³³, G.Smadja²⁵, N.Smirmov⁴², O.Smirmova²⁴, G.R.Smith³⁷, A.Sokolov⁴², O.Solovianov⁴², R.Sosnowski⁵¹, D.Souza-Santos⁶, T.Spaso²¹, E.Spiriti⁴⁰, P.Sponholz⁵², S.Squarcia¹³, D.Stampfer⁹, C.Stanescu⁴⁰, S.Stanic⁴³, S.Stapnes³³, I.Stavitski³⁶, K.Stevenson³⁵, A.Stocchi¹⁹, J.Strauss⁵⁰, R.Strub¹⁰, B.Stugu⁴, M.Szczekowski⁵¹, M.Szeptycka⁵¹, T.Tabarelli²⁸

J.P.Tavernet²³, F.Terranova²⁸, J.Thomas³⁵, A.Tilquin²⁷, J.Timmermans³¹, L.G.Tkatchev¹⁶, T.Todorov¹⁰, S.Todorova¹⁰, D.Z.Toet³¹, A.Tomaradze², B.Tome²¹, A.Tonazzo²⁸, L.Tortora⁴⁰, G.Transtromer²⁴, D.Treille⁹, G.Tristram⁸, A.Trombini¹⁹, C.Troncon²⁸, A.Tsirou⁹, M-L.Turluer³⁹, I.A.Tyapkin¹⁶, M.Tyndel³⁷, S.Tzamarias¹¹, B.Ueberschaer⁵², O.Ullaland⁹, V.Uvarov⁴², G.Valenti⁵, E.Vallazza⁹, C.Vander Velde², G.W.Van Apeldoorn³¹, P.Van Dam³¹, W.K.Van Doninck², J.Van Eldik³¹, A.Van Lysebetten², N.Vassilopoulos³⁵, G.Vegni²⁸, L.Ventura³⁶, W.Venus³⁷, F.Verbeure², M.Verlato³⁶, L.S.Vertogradov¹⁶, D.Vilanova³⁹, P.Vincent²⁵, L.Vitale⁴⁶, E.Vlasov⁴², A.S.Vodopyanov¹⁶, V.Vrba¹², H.Wahlen⁵², C.Walck⁴⁴, F.Waldner⁴⁶, P.Weilhammer⁹, C.Weiser¹⁷, A.M.Wetherell⁹, D.Wicke⁵², J.H.Wickens², M.Wielers¹⁷, G.R.Wilkinson⁹, W.S.C.Williams³⁵, M.Winter¹⁰, M.Witek¹⁸, T.Wlodek¹⁹, K.Woschnagg⁴⁸, K.Yip³⁵, O.Yushchenko⁴², F.Zach²⁵, A.Zaitsev⁴², A.Zalewska⁹, P.Zalewski⁵¹, D.Zavrtanik⁴³, E.Zevgolatakos¹¹, N.I.Zimin¹⁶, M.Zito³⁹, D.Zontar⁴³, G.C.Zucchelli⁴⁴, G.Zumerle³⁶

¹Department of Physics and Astronomy, Iowa State University, Ames IA 50011-3160, USA

²Physics Department, Univ. Instelling Antwerpen, Universiteitsplein 1, B-2610 Wilrijk, Belgium and IIHE, ULB-VUB, Pleinlaan 2, B-1050 Brussels, Belgium

and Faculté des Sciences, Univ. de l'Etat Mons, Av. Maistriau 19, B-7000 Mons, Belgium

³Physics Laboratory, University of Athens, Solonos Str. 104, GR-10680 Athens, Greece

⁴Department of Physics, University of Bergen, Allégaten 55, N-5007 Bergen, Norway

⁵Dipartimento di Fisica, Università di Bologna and INFN, Via Irnerio 46, I-40126 Bologna, Italy

⁶Centro Brasileiro de Pesquisas Físicas, rua Xavier Sigaud 150, RJ-22290 Rio de Janeiro, Brazil

and Depto. de Física, Pont. Univ. Católica, C.P. 38071 RJ-22453 Rio de Janeiro, Brazil

and Inst. de Física, Univ. Estadual do Rio de Janeiro, rua São Francisco Xavier 524, Rio de Janeiro, Brazil

⁷Comenius University, Faculty of Mathematics and Physics, Mlynska Dolina, SK-84215 Bratislava, Slovakia

⁸Collège de France, Lab. de Physique Corpusculaire, IN2P3-CNRS, F-75231 Paris Cedex 05, France

⁹CERN, CH-1211 Geneva 23, Switzerland

¹⁰Centre de Recherche Nucléaire, IN2P3 - CNRS/ULP - BP20, F-67037 Strasbourg Cedex, France

¹¹Institute of Nuclear Physics, N.C.S.R. Demokritos, P.O. Box 60228, GR-15310 Athens, Greece

¹²FZU, Inst. of Physics of the C.A.S. High Energy Physics Division, Na Slovance 2, 180 40, Praha 8, Czech Republic

¹³Dipartimento di Fisica, Università di Genova and INFN, Via Dodecaneso 33, I-16146 Genova, Italy

¹⁴Institut des Sciences Nucléaires, IN2P3-CNRS, Université de Grenoble 1, F-38026 Grenoble Cedex, France

¹⁵Helsinki Institute of Physics, HIP, P.O. Box 9, FIN-00014 Helsinki, Finland

¹⁶Joint Institute for Nuclear Research, Dubna, Head Post Office, P.O. Box 79, 101 000 Moscow, Russian Federation

¹⁷Institut für Experimentelle Kernphysik, Universität Karlsruhe, Postfach 6980, D-76128 Karlsruhe, Germany

¹⁸Institute of Nuclear Physics and University of Mining and Metallurgy, Ul. Kawiora 26a, PL-30055 Krakow, Poland

¹⁹Université de Paris-Sud, Lab. de l'Accélérateur Linéaire, IN2P3-CNRS, Bât. 200, F-91405 Orsay Cedex, France

²⁰School of Physics and Chemistry, University of Lancaster, Lancaster LA1 4YB, UK

²¹LIP, IST, FCUL - Av. Elias Garcia, 14-1º, P-1000 Lisboa Codex, Portugal

²²Department of Physics, University of Liverpool, P.O. Box 147, Liverpool L69 3BX, UK

²³LPNHE, IN2P3-CNRS, Universités Paris VI et VII, Tour 33 (RdC), 4 place Jussieu, F-75252 Paris Cedex 05, France

²⁴Department of Physics, University of Lund, Sölvegatan 14, S-22363 Lund, Sweden

²⁵Université Claude Bernard de Lyon, IPNL, IN2P3-CNRS, F-69622 Villeurbanne Cedex, France

²⁶Universidad Complutense, Avda. Complutense s/n, E-28040 Madrid, Spain

²⁷Univ. d'Aix - Marseille II - CPP, IN2P3-CNRS, F-13288 Marseille Cedex 09, France

²⁸Dipartimento di Fisica, Università di Milano and INFN, Via Celoria 16, I-20133 Milan, Italy

²⁹Niels Bohr Institute, Blegdamsvej 17, DK-2100 Copenhagen 0, Denmark

³⁰NC, Nuclear Centre of MFF, Charles University, Areal MFF, V Holesovickach 2, 180 00, Praha 8, Czech Republic

³¹NIKHEF, Postbus 41882, NL-1009 DB Amsterdam, The Netherlands

³²National Technical University, Physics Department, Zografou Campus, GR-15773 Athens, Greece

³³Physics Department, University of Oslo, Blindern, N-1000 Oslo 3, Norway

³⁴Dpto. Física, Univ. Oviedo, Avda. Calvo Sotelo, S/N-33007 Oviedo, Spain, (CICYT-AEN96-1681)

³⁵Department of Physics, University of Oxford, Keble Road, Oxford OX1 3RH, UK

³⁶Dipartimento di Fisica, Università di Padova and INFN, Via Marzolo 8, I-35131 Padua, Italy

³⁷Rutherford Appleton Laboratory, Chilton, Didcot OX11 0QX, UK

³⁸Dipartimento di Fisica, Università di Roma II and INFN, Tor Vergata, I-00173 Rome, Italy

³⁹CEA, DAPNIA/Service de Physique des Particules, CE-Saclay, F-91191 Gif-sur-Yvette Cedex, France

⁴⁰Istituto Superiore di Sanità, Ist. Naz. di Fisica Nucl. (INFN), Viale Regina Elena 299, I-00161 Rome, Italy

⁴¹Istituto de Física de Cantabria (CSIC-UC), Avda. los Castros, S/N-39006 Santander, Spain, (CICYT-AEN96-1681)

⁴²Inst. for High Energy Physics, Serpukov P.O. Box 35, Protvino, (Moscow Region), Russian Federation

⁴³J. Stefan Institute, Jamova 39, SI-1000 Ljubljana, Slovenia and Department of Astroparticle Physics, School of

Environmental Sciences, Kostanjevska 16a, Nova Gorica, SI-5000 Slovenia,

and Department of Physics, University of Ljubljana, SI-1000 Ljubljana, Slovenia

⁴⁴Fysikum, Stockholm University, Box 6730, S-113 85 Stockholm, Sweden

⁴⁵Dipartimento di Fisica Sperimentale, Università di Torino and INFN, Via P. Giuria 1, I-10125 Turin, Italy

⁴⁶Dipartimento di Fisica, Università di Trieste and INFN, Via A. Valerio 2, I-34127 Trieste, Italy

and Istituto di Fisica, Università di Udine, I-33100 Udine, Italy

⁴⁷Univ. Federal do Rio de Janeiro, C.P. 68528 Cidade Univ., Ilha do Fundão BR-21945-970 Rio de Janeiro, Brazil

⁴⁸Department of Radiation Sciences, University of Uppsala, P.O. Box 535, S-751 21 Uppsala, Sweden

⁴⁹IFIC, Valencia-CSIC, and D.F.A.M.N., U. de Valencia, Avda. Dr. Moliner 50, E-46100 Burjassot (Valencia), Spain

⁵⁰Institut für Hochenergiephysik, Österr. Akad. d. Wissensch., Nikolsdorfergasse 18, A-1050 Vienna, Austria

⁵¹Inst. Nuclear Studies and University of Warsaw, Ul. Hoza 69, PL-00681 Warsaw, Poland

⁵²Fachbereich Physik, University of Wuppertal, Postfach 100 127, D-42097 Wuppertal, Germany

⁵³On leave of absence from IHEP Serpukhov

1 Introduction

The W-boson mass, m_W , is one of the key parameters of the electroweak theory. The combined measurements at $p\bar{p}$ colliders give a value $m_W = 80.35 \pm 0.13 \text{ GeV}/c^2$ [1–5]. This is in agreement with the determination $m_W = 80.352 \pm 0.033 \text{ GeV}/c^2$ from a fit of all electroweak data to the Standard Model [6].

In 1996, LEP provided e^+e^- -collisions at a centre-of-mass energy of 161.31 GeV with an integrated luminosity recorded by DELPHI of 9.93 pb^{-1} , from which a measurement of the W-pair cross-section has been obtained. The cross-section for W-pair production near threshold depends strongly on m_W , which can therefore be determined from this measurement. It is also sensitive to the trilinear gauge coupling parameters (TGCs) at the WWV (*i.e.* WW γ and WWZ) vertices, and can therefore be used to set limits on these parameters if another measurement of m_W is used. Limits on TGCs have previously been obtained in $p\bar{p}$ experiments [7].

The paper is organized as follows. In section 2, the DELPHI detector setup in 1996, the event trigger, and the luminosity measurement are briefly reviewed. The track selection and lepton identification are described in section 3. In section 4, the event selection and the computation of cross-sections are presented for the different decay channels, from which a total cross-section is obtained. In section 5, a value for m_W is derived. Limits on TGCs are given in section 6.

2 Apparatus, Trigger and Luminosity

Detailed descriptions of the DELPHI apparatus and its performance can be found in [8,9]. In 1996 the cylindrical 3-layer vertex detector was lengthened and extended with additional silicon detectors covering the endcap region.

The response of the detector to various physics processes was modelled using the full simulation program DELSIM [9,10], which incorporates the resolution, granularity, and efficiency of the detector components. The event generators chosen are described in the relevant sections below.

The event trigger is described in [8,9]. From trigger efficiencies measured for single charged particles with redundant trigger combinations, the efficiency for two charged particles (which is the worst case for all events of interest in the present analysis) was found to exceed 99%.

The luminosity was measured using the Small Angle Tile Calorimeter (STIC). It consists of two lead/scintillator sampling calorimeters, located at $\pm 220 \text{ cm}$ from the interaction point, providing full coverage of the region between 29 and 185 mrad with respect to the beam axis. A detailed description of this detector can be found in [11]. Events corresponding to Bhabha scattering were selected by requiring a coincidence of two coplanar electromagnetic showers, each with energy larger than 65% of the beam energy. In order to minimize the sensitivity to the position of the interaction point, asymmetric cuts were imposed on the reconstructed radii of the two showers.

The calculation of the accepted cross-section was based on the event generator BHLUMI 4.03 [12], which has a theoretical accuracy of 0.25% at LEP2 energies. The generated events were passed through a full simulation of the detector, and analysed in the same way as the real data. The total experimental systematic error on the luminosity amounts to 0.5%, with the main contribution arising from the uncertainty in the radial cuts. For the data sample used, an integrated luminosity of $9.93 \pm 0.11(\text{stat.}) \pm 0.06(\text{syst.}) \text{ pb}^{-1}$ was determined.

3 Track Selection and Lepton Identification

Charged particles were selected if they fulfilled the following criteria :

- polar angle with respect to the beam direction between 10° and 170° ;
- momentum greater than $0.4 \text{ GeV}/c$;
- good quality, assessed as follows:
 - track length greater than 15 cm ;
 - impact parameters with respect to the nominal interaction point less than 4 cm (transverse and longitudinal with respect to the beam direction);
 - estimated relative error on momentum measurement less than 100% .

For neutral particles the following selection criteria were applied :

- energy of the shower greater than 0.5 GeV ;
- additional requirements on shower quality, assessed as follows:
 - showers in the STIC calorimeter with deposits in more than one cell;
 - showers in the hadron calorimeter with energy uncertainties below 100% .

Electron identification was performed in the polar angle range between 20° and 160° by looking for characteristic energy deposition in the central and forward/backward electromagnetic calorimeters and demanding an energy-to-momentum ratio consistent with unity. For this polar angle range the identification efficiency for high momentum electrons was determined from simulation to be $(77 \pm 2)\%$, in good agreement with efficiencies determined using Bhabha events measured in the detector.

Tracks were identified as due to muons if they had at least one associated hit in the muon chambers, or an energy deposition in the hadronic calorimeter consistent with a minimum ionizing particle. Muon identification was performed in the polar angle range between 10° and 170° . Within this acceptance, the identification efficiency was determined from simulation to be $(92 \pm 1)\%$. Good agreement was found between data and simulation for high momentum muons in $Z \rightarrow \mu^+ \mu^-$ decays, and for low momentum pairs produced in $\gamma\gamma$ reactions.

4 Event Selection and Cross-Sections

The cross-sections determined in this analysis are defined to correspond to W pair production through the three doubly resonant tree-level diagrams (“CC03 diagrams” [13]) involving s -channel γ and Z exchange and t -channel ν exchange. The selection efficiencies given in this section are also defined with respect to these diagrams only. Depending on the decay mode of each W, final states which are fully hadronic, mixed hadronic-leptonic (“semileptonic”), or fully leptonic are obtained with branching ratios derived from the Standard Model of 45.9% , 43.7% and 10.4% respectively. In addition to their production via the CC03 diagrams, the four-fermion final states corresponding to these decay modes may be produced via other electroweak diagrams involving either zero, one, or two massive vector bosons. The effects of the interference between the CC03 diagrams and the additional diagrams have been treated as correction factors, which were applied such that the cross-sections given below can be compared to theoretical estimates of the CC03 cross-sections. The correction factors C_{CC03} were determined for the individual decay modes using the 4-fermion generator EXCALIBUR [14], which is interfaced to the DELPHI simulation package [10], and are given in table 1. The uncertainties are

estimated to be about 1.5% and are taken into account in the systematic uncertainties on the cross-sections given below.

WW decay mode	C_{CC03}
$q\bar{q}q\bar{q}$	0.996
$e\nu q\bar{q}$	1.087
$\mu(\tau)\nu q\bar{q}$	1.006
$\ell\nu\ell\nu$	1.045

Table 1: Correction factors C_{CC03} for the decay modes of WW pairs. For $\ell\nu\ell\nu$ the correction factor given is the average of all lepton combinations.

4.1 Fully Hadronic Final State

The event selection criteria were optimised in order to ensure that the final state was purely hadronic and in order to reduce the residual background. The background is dominated by electron-positron annihilation into $q\bar{q}(\gamma)$, with a cross-section about two orders of magnitude larger than that for the signal.

For each event, all particles were clustered into jets using the LUCLUS algorithm [15] with $d_{join} = 6.5$ GeV/ c . At least 4 jets were required, with at least four particles in each jet. Figure 1a shows the distributions of the differential 3-jet rate as a function of d_{join} for data and for simulated WW and background events.

Events coming from the radiative return to the Z peak were rejected by requiring the effective centre-of-mass energy of the e^+e^- annihilation to be larger than 115 GeV. The effective energy was estimated from the momentum of the radiated photon. If an isolated photon was recorded in the detector, its measured momentum was used; otherwise its direction was assumed to be parallel to the beam axis, and its momentum was calculated by forcing a 2-jet interpretation of the event and then using only the angular information of the jets [16]. Figure 1b shows the distributions of the effective energy for events with at least 4 jets.

Events were then forced into a 4-jet configuration, and a kinematically constrained fit performed, imposing energy and momentum conservation. The final cut to separate WW from $q\bar{q}(\gamma)$ events was made on the variable

$$D = \frac{E_{min}}{E_{max}} \cdot \frac{\theta_{min}}{(E_{max} - E_{min})},$$

where E_{min}, E_{max} are the energies of the jets with least and greatest energy, and θ_{min} is the smallest interjet angle, after the constrained fit.

The D variable discriminates well between the signal and the $q\bar{q}(\gamma)$ background, for the following reason. The signal, with both W's on or near mass-shell, consists of events with two pairs of (nearly) back-to-back di-jets, the two di-jets being able to have any orientation with respect to each other and each jet having an energy in the range of about 30-50 GeV. In contrast, in $q\bar{q}gg$ background events the quarks tend to have higher energy than the radiated gluons, and the gluons tend to follow the quark directions. D was required to exceed 0.013 GeV $^{-1}$. Figure 1c shows the distributions of this quantity after the other two cuts described above.

The selection efficiency was computed from a sample of WW events generated with the generator PYTHIA 5.7 [17] (with $m_W = 80.23$ GeV/ c^2), with the fragmentation tuned

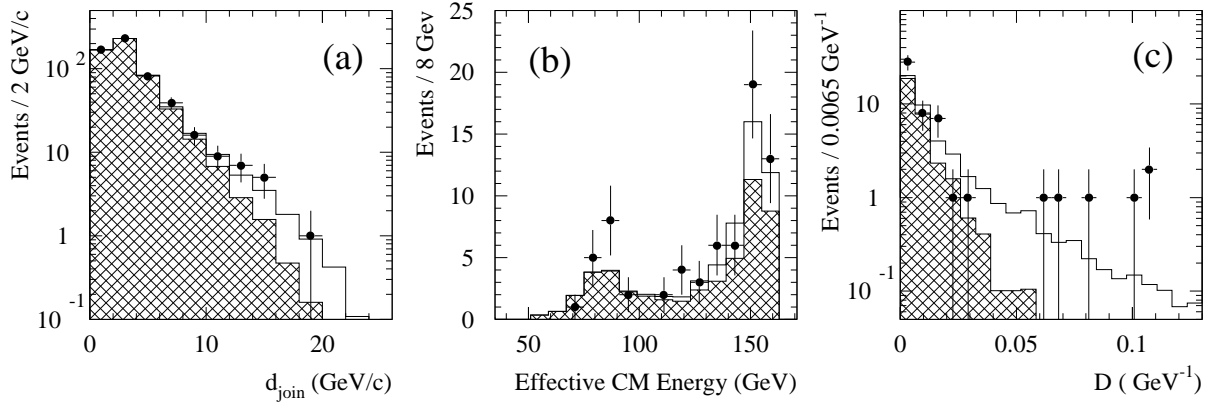


Figure 1: Fully hadronic final state: comparison of data (points with error bars) with simulated $q\bar{q}(\gamma)$ background (cross-hatched areas) and WW signal (white areas) normalised to the fitted cross-section. (a) Differential 3-jet rate (number of events changing from 4 to 3 jets) as function of d_{join} ; (b) effective centre-of-mass energy for events with at least 4 jets; (c) D variable (as defined in the text) for 4-jet events with effective centre-of-mass energy greater than 115 GeV.

to the DELPHI data measured at LEP1 [18], and was found to be $(61.3 \pm 2.0)\%$. The error includes the systematic uncertainty, which was estimated by varying all selection criteria by at least the value of their experimental resolutions and taking the quadratic sum of all contributions.

A residual background cross-section of 0.61 ± 0.07 pb was estimated, with the dominant contribution coming from e^+e^- annihilation into $q\bar{q}(\gamma)$ events, 0.4% of which survived the WW selection procedure, corresponding to a residual cross-section of 0.58 pb. The other contributions come from the channels $e^+e^- \rightarrow ZZ$ (0.02 pb) and $e^+e^- \rightarrow Ze^+e^-$ (0.01 pb). The systematic uncertainty on the background was estimated from the variation of the selection efficiency for the $q\bar{q}(\gamma)$ background using different generators. Furthermore the accuracy of the simulation was checked on multihadronic events collected at the Z pole and at collision energies between 130 and 140 GeV. These data were selected with the 161 GeV criteria downscaled in proportion to the collision energy, and good agreement was found for the expected numbers of selected events.

From the full data sample, 15 events were selected. An unbinned maximum likelihood fit to the distribution of the variable D , taking into account the expected background, leads to a cross-section for fully hadronic events

$$\sigma_{WW}^{4jet} = \sigma_{WW}^{tot} \times \text{BR}(WW \rightarrow 4 \text{ jets}) = 1.56_{-0.55}^{+0.67} \pm 0.13 \text{ pb},$$

where $\text{BR}(WW \rightarrow 4 \text{ jets})$ is the probability for the WW pair to give a purely hadronic final state, and the first errors are statistical and the last is systematic. The effects of colour reconnection are estimated to be negligible [19].

4.2 Semileptonic Final States

Events in which one W decays into $\ell\nu$ and the other one into quarks are characterized by two hadronic jets, one energetic and isolated charged lepton, and missing momentum

resulting from the neutrino. The major backgrounds to these events come from radiative $q\bar{q}$ production and four-fermion final states containing two quarks and two charged leptons of the same flavour. Photon conversions in the detector lead to an increase of background events in the electron channel.

Events were selected by requiring 6 or more charged particles and a missing momentum of more than 10 GeV/c. Electron and muon tagging were applied to the events. In $q\bar{q}(\gamma)$ events, the selected lepton candidates are either leptons produced in heavy quark decays, misidentified hadrons, or electrons from a materialized photon. These particles generally have low momenta and small angles with respect to their quark jets. Therefore the momentum of the selected muon or the energy deposited in the electromagnetic calorimeters by the selected electron was required to be greater than 10 GeV, and the angle θ_{iso} between the lepton and the nearest charged particle with a momentum greater than 1 GeV/c was required to be larger than 10° . For leptons with momenta less than 20 GeV/c, θ_{iso} was required to be larger than 30° . Figures 2a and 2b show the distributions of the isolation angle of the lepton and of its momentum. If more than one identified lepton passed these selections, the one of highest momentum was considered as the lepton candidate from the W decay. The angle between the lepton and the missing momentum vector was required to exceed 90° for electrons and 60° for muons. All other particles were forced into two jets using the LUCLUS algorithm [15]. Both jets had to contain at least one charged particle, and the event was rejected if the invariant mass of the jets was smaller than 30 GeV/c², or if the angle between the jets was smaller than 80° .

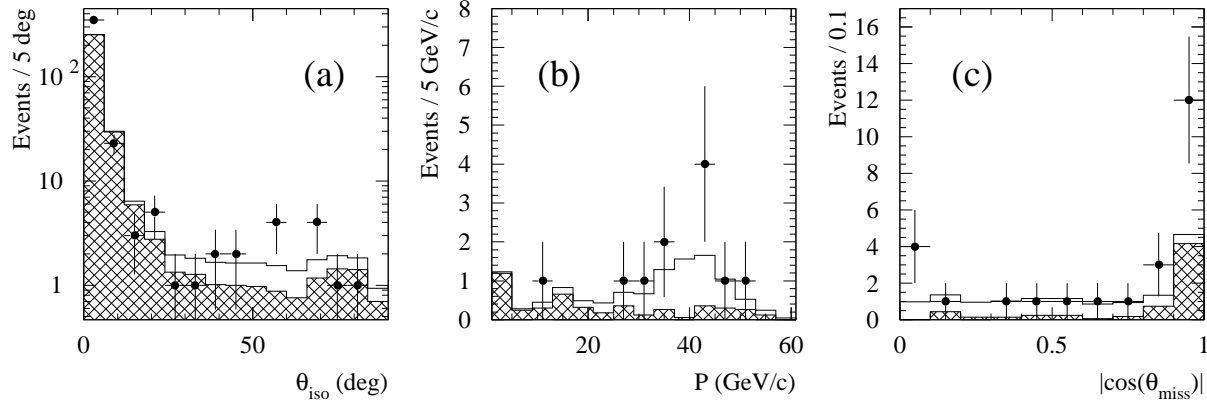


Figure 2: Semileptonic final state: (a) isolation angle of the lepton; (b) momentum of the lepton; (c) polar angle of the missing momentum. The full lines are the expectations for the fitted signal (white areas) plus the calculated background (cross-hatched areas); data points are shown with statistical error bars. Distribution (a) contains all events with at least 6 charged tracks and a lepton with momentum above 10 GeV/c; for (b) and (c), all selection criteria are applied except the one on the variable described by each plot.

The radiative $q\bar{q}(\gamma)$ background was suppressed further by looking for evidence of an initial state radiation (ISR) photon. Events were removed if there was an energy deposition cluster of above 20 GeV in the electromagnetic calorimeters, unassociated with a charged particle. Events with undetected ISR photons close to the beam direction were suppressed by requiring the polar angle of the missing momentum vector to exceed 20° for lepton momenta above 20 GeV/c, or else to exceed 32° . Figure 2c shows the polar angle distributions of the missing momentum. In addition, for $e\nu q\bar{q}$ events the component

of the missing momentum transverse to the beam axis, p_{miss}^T , had to exceed 10 GeV/ c , and the angles between the missing momentum vector and the directions of both jets had to exceed 10° for electrons in the polar angle range between 40° and 140° and to exceed 20° outside this range.

Four-fermion neutral current backgrounds ($q\bar{q}\ell\ell$) were reduced by applying an additional cut to events in which a second lepton of the same flavour and with charge opposite to that of the first was selected: the energy in a 10° cone around the second lepton direction was required to exceed 5 GeV.

If no identified lepton was found, the most energetic particle which formed an angle greater than 25° with all other charged particles was considered as the lepton candidate; this recovered unidentified leptons and some additional $W \rightarrow \tau\nu_\tau$ decays. In this case a momentum greater than 20 GeV/ c was required, and tighter cuts were also applied to the magnitude of the missing momentum (required to be above 20 GeV/ c), to its polar angle (above 32°), and to its angles to both jets (above 20°).

To improve the selection of $W \rightarrow \tau\nu_\tau$ decays, events with at least 6 charged particles were selected if they showed a 3-jet topology for $d_{join} > 4.0$ GeV/ c . A missing momentum above 10 GeV/ c with polar angle above 20° was required, and the missing energy had to exceed 45 GeV. One jet had to be τ -like, *i.e.* to have :

- charged multiplicity between 1 and 3;
- total multiplicity less than 5;
- total energy above 8 GeV;
- fraction of charged energy above 0.1;
- fraction of the jet energy in a cone of 5° around the jet axis above 0.7.

The angle between this jet and the missing momentum vector had to exceed 90° . In order to reduce the background from $q\bar{q}(\gamma)$ events further, additional cuts on the invariant mass of the two other jets ($m_{jj} > 40$ GeV/ c^2), on the angle between them ($\cos\theta_{jj} < -0.8$), and on their angle with the missing momentum vector (above 20°) were imposed. In addition, events were rejected if the effective centre-of-mass energy of the e^+e^- annihilation (see section 4.1) was above 150 GeV or in the range of the Z resonance (80-100 GeV).

The efficiency for selecting the signal ($WW \rightarrow \ell\nu jj$) was calculated using events simulated with PYTHIA 5.7 to be $(60.9 \pm 3.0)\%$. The cross-section for background events which pass all selection criteria was evaluated using different generators to be 0.193 ± 0.024 pb, with the main contributions coming from the channels $e^+e^- \rightarrow q\bar{q}(\gamma)$ (0.127 pb) and $e^+e^- \rightarrow Ze^+e^-$ (0.041 pb). The errors on signal efficiency and background include all systematic uncertainties, where the error on the background is dominated by hadron misidentification and photon conversions.

From a data sample corresponding to an integrated luminosity of 9.69 pb $^{-1}$, 12 events were selected. From this the WW cross-section for semileptonic decays was derived to be

$$\sigma_{WW}^{\ell\nu jj} = \sigma_{WW}^{tot} \times \text{BR}(WW \rightarrow \ell\nu jj) = 1.77_{-0.55}^{+0.67} \pm 0.10 \text{ pb},$$

where the first errors are statistical and the last is systematic.

4.3 Fully Leptonic Final States

Events in which both W-bosons decay into $\ell\nu$ are characterized by two energetic, acollinear and acoplanar leptons of opposite charge, and by large missing energy and momentum. In $W \rightarrow \mu\nu$ and $W \rightarrow e\nu$ decays, the energy of the lepton ranges typically between 20 and 60 GeV; $W \rightarrow \tau\nu$ decays produce either a single charged particle with

a lower momentum, or a narrow jet. The relevant backgrounds are dilepton events from $e^+e^- \rightarrow Z(\gamma)$, Bhabha scattering, and two-photon collisions.

In order to select a sample of purely leptonic events, a charged particle multiplicity between 2 and 6 was required, with the total energy of these particles greater than 40 GeV. All particles in the event were then clustered into jets using the LUCLUS algorithm [15] with $d_{join} = 5.0$ GeV/ c . The following selection was then applied to the jet variables, thus including hadronic tau decays in the sample: a) only events with two reconstructed jets were retained, b) the momentum of the leading jet was required to be between 20 and 60 GeV/ c and that of the other jet between 12 and 50 GeV/ c . Events with detected hard photons, such as those from radiative Z production with the ISR photon entering the detector acceptance, were explicitly rejected by requiring there to be no electromagnetic calorimeter cluster with energy above 30 GeV and unassociated with a charged particle.

An acollinearity $\theta_{acol} > 10^\circ$ and acoplanarity $\theta_{apl} > 10^\circ$ were required; the former suppresses non-radiative di-lepton production, the latter is also effective against radiative background events. Cuts on the minimum polar angle of the two jets (θ between 20° and 160°) and on the direction of the missing momentum ($|\cos \theta_{miss}| < 0.94$) further reduced the backgrounds due to two-photon collisions and Bhabha scattering, which are concentrated at low polar angles. Figure 3 shows the distribution of the momentum spectrum of the leading jet and of the acoplanarity.

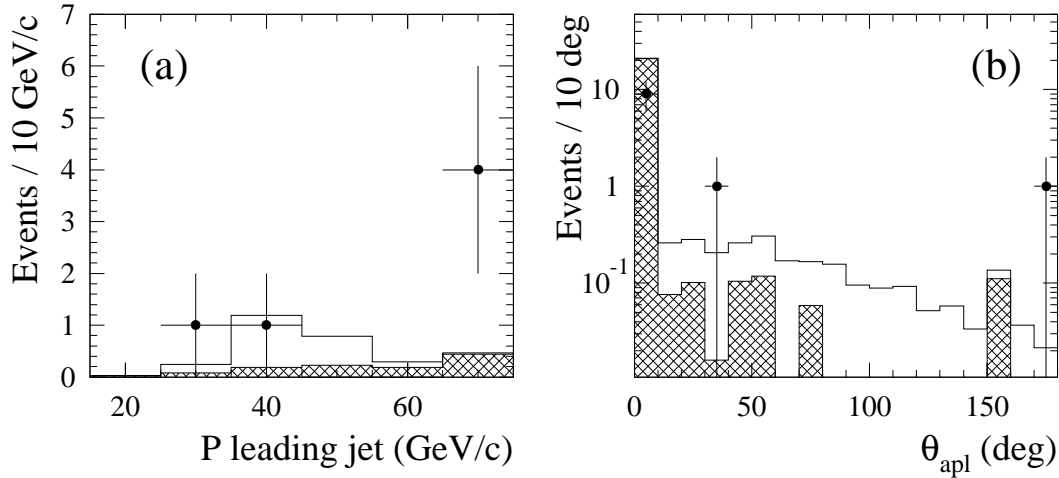


Figure 3: Fully leptonic final states: (a) momentum of the leading jet; (b) acoplanarity. The full lines are the expectations for the fitted signal (white areas) plus the calculated background (cross-hatched areas), the data points are shown with statistical error bars. All cuts are applied except the one on the variable described by each plot.

The global efficiency of these selection criteria was computed to be $(47.7 \pm 3.0)\%$; it is considerably higher for events in which neither of the W-bosons decays to a tau lepton. The total cross-section for background events which pass all the selection cuts was computed from simulated events to be 0.06 ± 0.04 pb. The errors contain the estimated systematic uncertainties.

With the criteria described above, 2 events were selected in the full data sample. The cross-section for purely leptonic final states was determined to be

$$\sigma_{\text{WW}}^{\ell\nu\ell\nu} = \sigma_{\text{WW}}^{\text{tot}} \times \text{BR}(\text{WW} \rightarrow \ell\nu\ell\nu) = 0.31^{+0.39}_{-0.24} \pm 0.09 \text{ pb},$$

where the first errors are statistical and the last is systematic.

4.4 Total Cross-section

The total cross-section for WW production was obtained from a likelihood fit based on the product of the probabilities of finding the observed number of events in each final state, using the branching fractions for each of them derived from the Standard Model, giving:

$$\sigma_{\text{WW}}^{\text{tot}} = 3.67^{+0.97}_{-0.85} \pm 0.19 \text{ pb},$$

where the first errors are statistical and the last is systematic. Similar results were obtained by the other LEP experiments [21].

5 Determination of the Mass of the W-boson

As mentioned in Section 1, the cross-section for $e^+e^- \rightarrow W^+W^-$ near threshold is very sensitive to the value of m_W , and its measured value can therefore be used to estimate m_W . Such an estimate is, of course, strictly valid only within the Standard Model.

In the previous section the total cross-section for $\sigma(e^+e^- \rightarrow W^+W^-)$ has been determined. As mentioned in section 4, the approach adopted here has been to correct the data to correspond to a CC03 cross-section. This procedure involves several theoretical uncertainties arising from the treatment of the finite W-boson width, the uncertainty in the Coulomb term (this term, representing the Coulomb force between the W pair, is important near threshold), and from uncertainties in other radiative corrections. These effects have been considered in detail in [13], where it is concluded that the present theoretical uncertainty on the CC03 cross-section computation is about $\pm 2\%$. This corresponds to an uncertainty on m_W of $\pm 0.04 \text{ GeV}/c^2$. In this paper the program used for the CC03 computation was that taken from reference [20]. As a cross-check, the result was compared to that obtained using reference [22] and the calculations with the default settings in the programs were found to agree at the level of 1%.

In addition, it was verified that the selection efficiency does not depend strongly on the precise value of m_W . This study was performed at generator level, using the EXCALIBUR generator, with cuts applied which emulated those applied to the data. Both for the CC03 subset of diagrams, and for all diagrams, the efficiency was found to be independent of m_W within the range 80.1 to 80.6 GeV/c^2 to within the statistical accuracy of the generated samples (about 1.5%).

The mean LEP beam energy was determined using a model based on the field readings of nuclear magnetic resonance probes installed in the dipole magnets. The probes were calibrated with resonant depolarisation measurements at $\sqrt{s} \approx m_Z$ [†]. A cross-check of the energy scale was made using flux-loop measurements. The effect of the RF system at the DELPHI interaction point was modelled, and a mean correction of 9 MeV was applied to the centre-of-mass energy. From these studies the LEP luminosity-weighted average centre-of-mass energy at DELPHI, E_{CM} , was determined to be [23]

$$E_{CM} = 161.31 \pm 0.05 \text{ GeV},$$

[†]The presence of machine imperfections inhibits the build up of transverse polarization at energies significantly higher than 50 GeV, so the resonant depolarisation technique cannot be used at the WW threshold.

where the error accounts for the calibration of the nuclear magnetic resonance probes at high energy, the understanding of the RF system, and additional smaller effects.

From the value of the cross-section given in section 4.4, $\sigma_{\text{WW}}^{\text{tot}} = 3.67^{+0.97}_{-0.85} \pm 0.19$ pb, the value of the W-boson mass was then determined to be

$$m_{\text{W}} = 80.40 \pm 0.44 \text{ (stat.)} \pm 0.09 \text{ (syst.)} \pm 0.03 \text{ (LEP)} \text{ GeV}/c^2,$$

where the first error is from the statistical uncertainty on the cross-section, the systematic error includes both the experimental systematic errors and the theory error discussed above, and the LEP error comes from the uncertainty on the centre-of-mass energy. Figure 4 shows the dependence of the WW cross-section at 161.31 GeV on m_{W} together with the DELPHI result.

A further check of the method was made by evaluating m_{W} in a pure four-fermion analysis, using EXCALIBUR to calculate cross-sections and to generate events which were passed through the DELPHI simulation program for efficiency determinations. Consistent results were obtained.

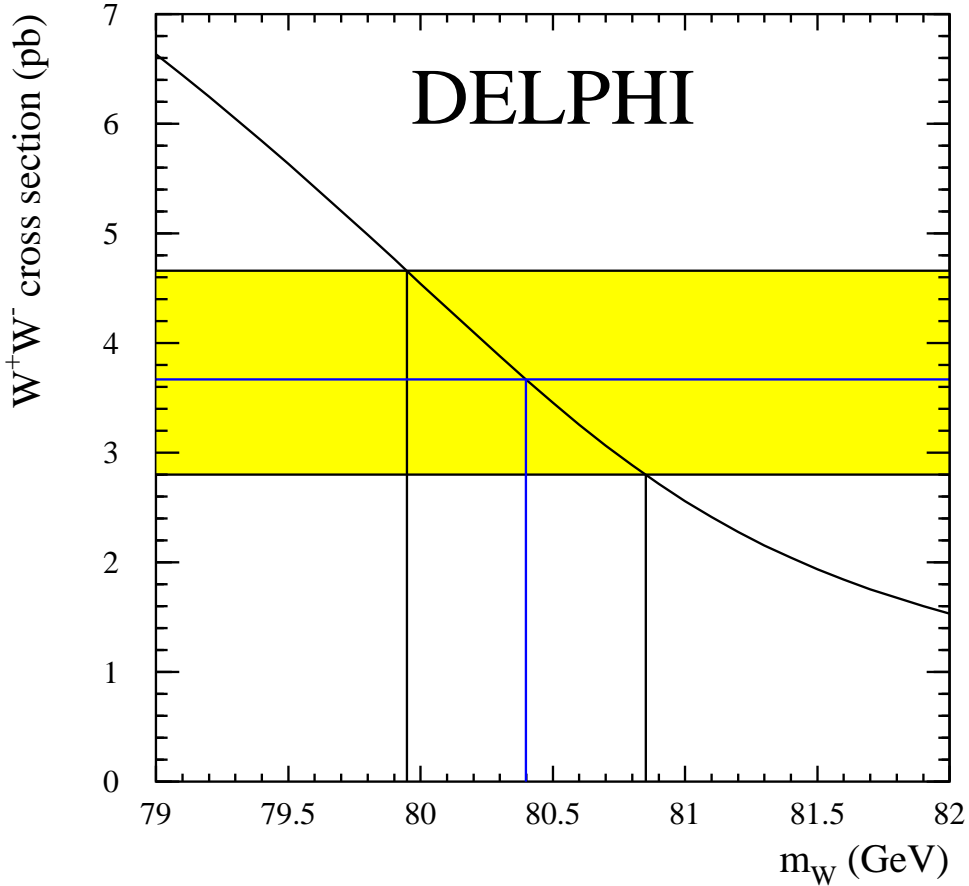


Figure 4: Cross-section for $e^+e^- \rightarrow W^+W^-$ at 161.31 GeV versus m_{W} with the DELPHI result. The shaded band corresponds to a 1 s.d. variation of the measured cross-section.

6 Determination of Limits on Trilinear Gauge Couplings

If m_W is taken to have the value of 80.35 ± 0.13 GeV/ c^2 [5] determined in $p\bar{p}$ experiments, the WW threshold cross-section can be used to provide limits on possible non-standard couplings at the WWV vertices. Here we interpret our measurement in terms of two such couplings.

The first is $\alpha_{W\phi}$, the contribution from one of the three CP -conserving components of dimension 6 in the Lagrangian \mathcal{L}_{WWV} which satisfy $SU(2) \times U(1)$ invariance and are not excluded by previous measurements. According to the relations given in [24], a non-zero value of $\alpha_{W\phi}$ would imply non-standard values of the dipole couplings κ_γ and κ_Z and of the WWZ coupling g_Z .

The second is $\tilde{\alpha}_W$, a possible CP -violating quadrupole contribution defined in [25]. The relation between this TGC and the CP -violating couplings in other commonly used schemes can be found in [25,26]. In particular, a non-zero value of $\tilde{\alpha}_W$ would imply non-zero values of the couplings $f_6^{\gamma,Z}$ which, as pointed out in [27], are not subject to the same kinematic suppression at the WW threshold as all the other couplings (both CP -conserving and CP -violating). It is therefore of considerable interest to use these data to impose limits on a possible contribution from this source.

The amplitudes contributing to the WW production process depend linearly on the TGCs α_i ($\equiv \alpha_{W\phi}, \tilde{\alpha}_W$); the cross-section therefore has a quadratic dependence on any one TGC, which may be used in comparison with the observed production rate to derive limits on any non-standard contribution. The dependences of the cross-section on the α_i considered here are such that their minima occur close to the Standard Model value, $\alpha_i = 0$.

The number of events in each of the three channels considered in section 4 (hadronic, semileptonic and fully leptonic) is given as a function of α_i by:

$$N_j(\alpha_i) = \mathcal{L} \cdot \{ \epsilon_j^s(\alpha_i) \sigma_j^s(\alpha_i) + \epsilon_j^b \sigma_j^b \}, \quad (1)$$

where \mathcal{L} represents the integrated luminosity, and the ϵ_j represent the experimental efficiencies in channel j determined in the four-fermion analysis mentioned in the previous section, the superscripts s and b denoting signal and background respectively. The predicted variation with the α_i of the $N_j(\alpha_i)$ was evaluated using the four-fermion generators ERATO [28] and EXCALIBUR [14], to take the interference terms between doubly resonant and other diagrams discussed in the previous section correctly into account. Separate calculations using these two generators yielded compatible predictions for the cross-sections. The probabilities of seeing 15, 12 and 2 events in the hadronic, semileptonic and fully leptonic channels, respectively, when $N_j(\alpha_i)$ are expected were evaluated and then combined in maximum likelihood fits of the α_i , giving limits at 95% confidence level of

$$\begin{aligned} -1.9 &< \alpha_{W\phi} < +2.0 \quad , \\ -1.1 &< \tilde{\alpha}_W < +1.3 \quad . \end{aligned}$$

The effects of systematic errors were studied by convoluting the probability function described above with Gaussian distributions of the relevant parameters and repeating the fits. They have been included in the results given. The dominant systematic effect comes from the uncertainty in m_W ; this leads to a broadening of the regions accepted in $\alpha_{W\phi}$ and in $\tilde{\alpha}_W$ by ≤ 0.04 at each end. Smaller systematic errors come from uncertainties

in estimates of selection efficiencies and from the statistical errors in the calculation of background cross-sections, and from the uncertainty in the LEP energy.

7 Summary

From an integrated luminosity of 9.93 pb^{-1} accumulated by DELPHI at an energy of 161.31 GeV, the W-pair cross-section has been determined in its various decay modes, giving a total cross-section

$$\sigma_{\text{WW}}^{\text{tot}} = 3.67_{-0.85}^{+0.97} \text{ (stat.)} \pm 0.19 \text{ (syst.) pb.}$$

From these measurements, assuming Standard Model couplings, the value of the W mass has been determined to be

$$m_{\text{W}} = 80.40 \pm 0.44 \text{ (stat.)} \pm 0.09 \text{ (syst.)} \pm 0.03 \text{ (LEP) GeV}/c^2 \text{ ,}$$

in agreement with previous measurements [1–5] and with a fit of electroweak data to the Standard Model [6].

Alternatively, by assuming m_{W} to be fixed at its current experimentally determined value, we have derived 95% confidence limits on TGCs of

$$\begin{aligned} -1.9 &< \alpha_{\text{W}\phi} < +2.0 \text{ ,} \\ -1.1 &< \tilde{\alpha}_{\text{W}} < +1.3 \text{ .} \end{aligned}$$

where each limit is derived assuming that the other TGCs are fixed at their Standard Model values, and the limits include estimates of the effects of systematic errors.

Acknowledgements

We thank the SL division of CERN for the excellent performance of the LEP collider and their careful work on the beam energy determination. We are also grateful to the technical and engineering staffs in our laboratories and to our funding agencies for their continuing support. It is a pleasure to thank Costas Papadopoulos for illuminating conversations on four-fermion physics.

References

- [1] UA2 Collaboration: J. Alitti et al., Phys. Lett. **B276** (1992) 354.
- [2] CDF Collaboration: F. Abe et al., Phys. Rev. Lett. **65** (1990) 2243;
CDF Collaboration: F. Abe et al., Phys. Rev. **D43** (1991) 2070.
- [3] CDF Collaboration: F. Abe et al., Phys. Rev. Lett. **75** (1995) 11.
- [4] D0 Collaboration: S. Abachi et al., Phys. Rev. Lett. **77** (1996) 3309.
- [5] M.Rijssenbeek, *W mass from the Tevatron*, FERMILAB CONF-96/365-E, to appear in the proceedings of the 28th International Conference on High Energy Physics, Warsaw, 25-31 July 1996.
- [6] The LEP Collaborations, the LEP Electroweak Working Group and the SLD Heavy Flavor Group, *A Combination of Preliminary LEP and SLD Electroweak Measurements and Constraints to the Standard Model*, CERN-PPE 96-183 (1996).
- [7] CDF Collaboration: F. Abe et al., Phys. Rev. Lett. **74** (1995) 1936;
CDF Collaboration: F. Abe et al., Phys. Rev. Lett. **75** (1995) 1017;
D0 Collaboration: S. Abachi et al., Phys. Rev. Lett. **77** (1996) 3303;
D0 Collaboration: S. Abachi et al., *Limits on Anomalous WW γ Couplings from $p\bar{p} \rightarrow W\gamma + X$ Events at $\sqrt{s} = 1.8$ TeV*, Fermilab-Pub-96/434-E, hep-ex/9612002 (1996).
- [8] DELPHI Collaboration: P. Aarnio et al., Nucl. Instr. & Meth. **A303** (1991) 233.
- [9] DELPHI Collaboration: P. Abreu et al., Nucl. Instr. & Meth. **A378** (1996) 57.
- [10] DELPHI Collaboration: *DELPHI event generation and detector simulation - User Guide*, DELPHI Note 89-67 (1989), unpublished.
- [11] A. C. Benvenuti et al., *The DELPHI Small Angle Tile Calorimeter*, contribution to IEEE NSS 1994.
- [12] S. Jadach, O. Nicrosini et al., *Event Generators for Bhabha Scattering*, Physics at LEP2, eds. G. Altarelli, T. Sjöstrand and F. Zwirner, CERN 96-01 (1996) Vol 2, 229.
- [13] W. Beenakker, F. A. Berends et al., *WW Cross-Section and Distributions*, Physics at LEP2, eds. G. Altarelli, T. Sjöstrand and F. Zwirner, CERN 96-01 (1996) Vol 1, 79.
- [14] F. A. Berends, R. Kleiss, R. Pittau, *EXCALIBUR*, Physics at LEP2, eds. G. Altarelli, T. Sjöstrand and F. Zwirner, CERN 96-01 (1996) Vol 2, 23.
- [15] T. Sjöstrand, *PYTHIA 5.7 / JETSET 7.4*, CERN-TH.7112/93 (1993).
- [16] P. Abreu, D. Fassouliotis, A. Grefrath, R.P. Henriques and L. Vitale, *SPRIME, A Package for Estimating the Effective $\sqrt{s'}$ Centre of Mass Energy in $q\bar{q}(\gamma)$ Events*, internal DELPHI note 96-124 PHYS 632 (1996), unpublished.
- [17] T. Sjöstrand, *PYTHIA 5.719 / JETSET 7.4*, Physics at LEP2, eds. G. Altarelli, T. Sjöstrand and F. Zwirner, CERN 96-01 (1996) Vol 2, 41.
- [18] DELPHI Collaboration: P. Abreu et al., Z. Phys. **C73** (1996) 11.
- [19] W.J. Stirling, private communication.
- [20] D. Bardin et al., *GENTLE/4fan*, Physics at LEP2, eds. G. Altarelli, T. Sjöstrand and F. Zwirner, CERN 96-01 (1996) Vol 2, 26.
- [21] ALEPH Collaboration, paper in preparation;
L3 Collaboration, paper in preparation;
OPAL Collaboration, Phys. Lett. **B389** (1996) 416.
- [22] W.J. Stirling, Nucl. Phys. **B456** (1995) 3.
- [23] The working group for LEP energy, *LEP Energy Calibration in 1996*, LEP Energy Group/97-01 (1997).
- [24] G. Gounaris, J.-L. Kneur and D. Zeppenfeld, *Triple Gauge Boson Couplings*, Physics

- at LEP2, eds. G. Altarelli, T. Sjöstrand and F. Zwirner, CERN 96-01 (1996) Vol 1, 525.
- [25] G.J. Gounaris and C.G. Papadopoulos, *Studying trilinear gauge couplings at Next Linear Collider*, Democritos - Thessaloniki preprint DEMO-HEP 96/04, THES-TP 96/11, hep-ph/9612378 (1996).
- [26] K. Hagiwara, K. Hikasa, R. D. Peccei and D. Zeppenfeld, Nucl. Phys. **B282** (1987) 253.
- [27] V.C. Spanos and W.J. Stirling, *Constraining a CP-violating WWV coupling from the W^+W^- threshold cross section at LEP2*, Durham preprint DTP/96/54, hep-ph/9607420 (1996).
- [28] C.G. Papadopoulos, Phys. Lett. **B352** (1995) 144;
C.G. Papadopoulos, *ERATO: event generator for four fermion production at LEP2 energies and beyond*, DEMO-HEP-96/02, hep-ph/9609320 (1996), to appear in *Computer Physics Communications*.